


Singular Continuous and Nonreciprocal Phonons in Quasicrystal AlPdMn

Masato Matsuura^{1,*}, Jinjia Zhang², Yasushi Kamimura², Maiko Kofu³, and Keiichi Edagawa²¹*Neutron Science and Technology Center, Comprehensive Research Organization for Science and Society (CROSS), Tokai, Ibaraki 319-1106, Japan*²*Institute of Industrial Science, The University of Tokyo, Tokyo, Japan*³*J-PARC Center, Japan Atomic Energy Agency, Tokai, Japan* (Received 29 November 2023; revised 22 January 2024; accepted 5 August 2024; published 25 September 2024)

In quasicrystals lacking translational symmetry but having highly ordered structures, understanding how phonons propagate in their aperiodic lattices remains an unsolved issue. We present an inelastic neutron scattering study on acoustic phonon modes of icosahedral quasicrystal AlPdMn, revealing hierarchical pseudo-gap structure in low-energy acoustic modes. Additionally, phonon intensities are asymmetric in energy and wave vectors with respect to the Bragg peak, indicating characteristic nonreciprocal phonon propagation in quasicrystals.

DOI: [10.1103/PhysRevLett.133.136101](https://doi.org/10.1103/PhysRevLett.133.136101)

Since the discovery of aperiodic long-range order with noncrystallographic symmetry in an Al-Mn alloy [1], the physical properties peculiar to quasicrystals have been widely studied. Properties such as the high electrical resistivity compared to ordinary metals [2], excessive specific heat over Dulong-Petit's law [3], low thermal conductivity [4], robust quantum criticality [5], and superconductivity in quasicrystals [6] have been reported. To explain these peculiar features in quasicrystals, it is important to understand the static and dynamic nature of the aperiodic lattice. Although progress has been made in understanding the static structure of quasicrystals through higher-dimensional crystallography comprising physical and complementary spaces [7–9], knowledge of the dynamic response of quasicrystals is still limited.

In metals with periodic lattices, the band theory established based on Bloch's theorem shows a continuous electronic density of states. In contrast, in quasicrystals where descriptions by periodic Bloch functions break down owing to lack of translational symmetry, singular continuous states with spiky electronic density of states (DOS) and an infinite number of fine gaps were theoretically predicted [10]. Such fine gaps are also predicted in phonons at the so-called pseudo-Brillouin zone boundaries [11,12], whose wave vectors are defined by half wave vector of Bragg peaks. The singular continuous nature in phonons is related to a simple but fundamental question on the lattice dynamics in quasicrystals: how lattice waves propagate in nonperiodic but highly ordered structure. In quasicrystals without translational symmetry, Brillouin zones cannot be defined. Instead, pseudo-gaps are supposed to open in phonon spectra at pseudo-Brillouin zone boundaries. Since Q space is filled with an infinite number of Bragg peaks

due to self-similar structure of quasicrystals, phonons are expected to be scattered at infinite number of Q 's.

Early studies on phonons in quasicrystals by using inelastic neutron scattering observed normal acoustic modes without a clear pseudo-gap [13,14]. Later, a pseudo-gap was observed by using inelastic x-ray scattering in both i-ZnMgSc quasicrystal and ZnSc 1/1 approximant [15]. However, these pseudo-gaps were measured with relatively coarse energy (E) resolution (ΔE) of ~ 1 meV at reduced wave vectors from a Bragg point $q = Q - Q_{\text{Bragg}} = 0.5\text{--}0.7 \text{ \AA}^{-1}$, which corresponds to the wavelength (λ) of 10–12 Å. Both quasicrystal i-ZnMgSc and ZnSc approximants have similar local structures, a large rhombic triacontahedron unit with a radius of 7–8 Å. Therefore, aperiodic features may not appear clearly for the phonon with a short λ comparable to the size of the common local structure of quasicrystals and periodic approximant.

To identify lattice dynamics related to aperiodicity, this study focuses on acoustic phonon modes at low energies and a small q value as they reflect lattice dynamics on a larger scale owing to the linear dispersion relation $\hbar\omega \sim cq \sim 2\pi c/\lambda$, where $\hbar\omega$ and c are the excitation energy and velocity of phonons, respectively. By using state-of-the-art neutron time-of-flight spectrometers with various ΔE extending from 0.004 to 1.2 meV, corresponding to λ of $2\text{--}3 \times 10^4$ Å, we found hierarchical pseudo-gap structures in the acoustic mode with spiky phonon intensity as a function of energy. The pseudo-gap energies are scaled by golden mean $\tau = (1 + \sqrt{5})/2$, a crucial constant for the self-similar structure in the face-centered icosahedral quasicrystal lattice, indicating a close correlation to aperiodicity. Additionally, asymmetric signals were found both in energy and wave vectors in a distinct manner from the nonreciprocal phonons in periodic lattices [16].

*Contact author: m_matsuura@cross.or.jp

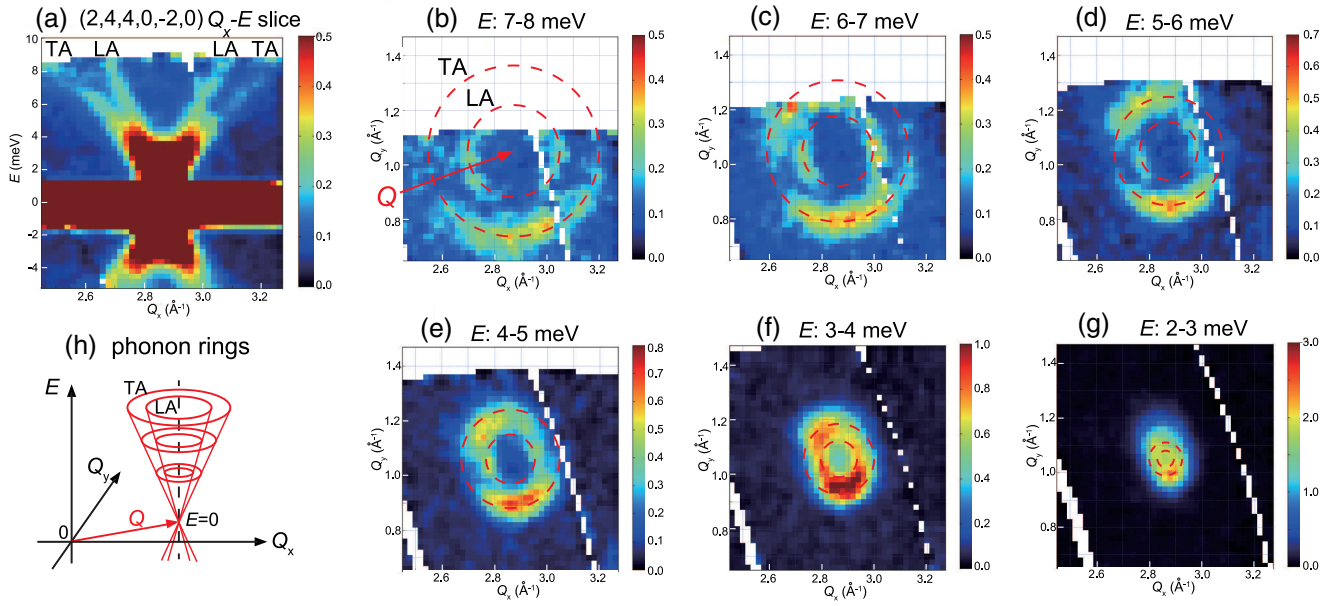


FIG. 1. Contour maps of phonon scattering intensity at a temperature of 300 K around the $(2, 4, 4, 0, -2, 0)$ Bragg peak centered at $(Q_x, Q_y, Q_z) = (2.86 \text{ \AA}^{-1}, 1.07 \text{ \AA}^{-1}, 0)$ obtained using the AMATERAS spectrometer with a coarse energy resolution of 1.2 meV. The Q_x - E slice in (a) integrates phonon intensities in the Q region of $|Q_z| < 0.1$ and $|Q_y - 1.07| < 0.1 \text{ \AA}^{-1}$, whereas the Q_x - Q_y slices in (b)–(g) integrate for $|Q_z| < 0.1 \text{ \AA}^{-1}$ and the energy width of 1 meV. (h) Schematic of phonon rings in the E - Q space.

Alloy ingots with a nominal composition of $\text{Al}_{73}\text{Pd}_{19}\text{Mn}_8$ were synthesized by arc melting under an argon atmosphere. A 16 mm- ϕ bulk single crystal of i-AlPdMn with a length of 24 mm and a mass of 12 g was grown using the Bridgman technique [17] (Fig. S1 in Supplemental Material [18]). The quasilattice constant was determined to be 9.175 \AA with single crystal x-ray diffraction measurements. Six-dimensional indices of Bragg peaks are given following the scheme of Elser [19]. Throughout this Letter, we label the momentum transfer in units of \AA^{-1} . Neutron scattering measurements were performed using a disk chopper spectrometer AMATERAS [20] and a near-backscattering time-of-flight spectrometer DNA [21] at the Materials and Life Science Experimental Facility, J-PARC. Neutron scattering data were obtained using the UTSUSEMI software [22].

Figure 1 shows the phonon spectra of i-AlPdMn around the Bragg peak $(2, 4, 4, 0, -2, 0)$ on the twofold axis obtained with a coarse ΔE of 1.2 meV. The location in the scattering plane and indices of the Bragg peak are described in Fig. S2 and Table S1 in Supplemental Material [18]. Two linear acoustic branches emerge from the Bragg peak [Fig. 1(a)]. The phonon signal forms rings in the two-dimensional $(Q_x$ - $Q_y)$ scattering plane [Figs. 1(b)–1(g)] as schematically shown in Fig. 1(h). In neutron scattering, the phonon scattering intensity is proportional to $(\mathbf{Q} \cdot \boldsymbol{\xi})^2$, where \mathbf{Q} and $\boldsymbol{\xi}$ are the wave vector and the polarization vector of the phonon mode, respectively. The intensity of the small (large) phonon rings in Figs. 1(b)–1(g) is strong in the direction parallel (perpendicular) to the Q vector, which

corresponds to longitudinal (transverse) acoustic phonons. The phonon rings shrink as energy decreases and no clear pseudo-gap structure was observed in the Q -integrated intensity with the coarse ΔE (Fig. S3 in Supplemental Material [18]), which is consistent with the previous reports [13–15,23].

Owing to the progress in modern pulsed neutron spectrometers, fine phonon spectra can now be obtained with approximately 10 times better ΔE (0.15 meV) compared to the previous reports [13–15,23]. Figure 2 shows the phonon spectra around the Bragg peak $(0, 2, 2, 0, -2, 0)$ on the three-fold axis obtained with the better energy resolution. The Q_x - E slice [Fig. 2(a)] shows that the phonon intensity drops discontinuously at several energies. Although the phonon intensity is distributed in specific directions, the averaged phonon rings in Figs. 2(b)–2(g) linearly shrink as the energy decreases similar to those around $(0, 2, 2, 0, -2, 0)$ [see dispersions in Fig. 2(h)], thereby indicating the same origin of these signals as those of the TA and LA phonons in Fig. 1.

To depict the energy dependence of phonon intensity, Fig. 3(a) shows the Q -integrated phonon intensity around $(0, 2, 2, 0, -2, 0)$. In general, the intensity of acoustic modes in periodic lattices increases inversely proportional to energy. However, the acoustic mode for the quasicrystal exhibits abrupt drops in intensity at several energies: 0.5–1.1, 1.3–1.75, and 2.2 meV. Here, we define a pseudo-gap as an energy region where a phonon intensity of an acoustic mode shows a dip structure. As the temperature (T) increases from 300 to 500 K, the intensities in between these pseudo-gaps are enhanced, indicating the phononic

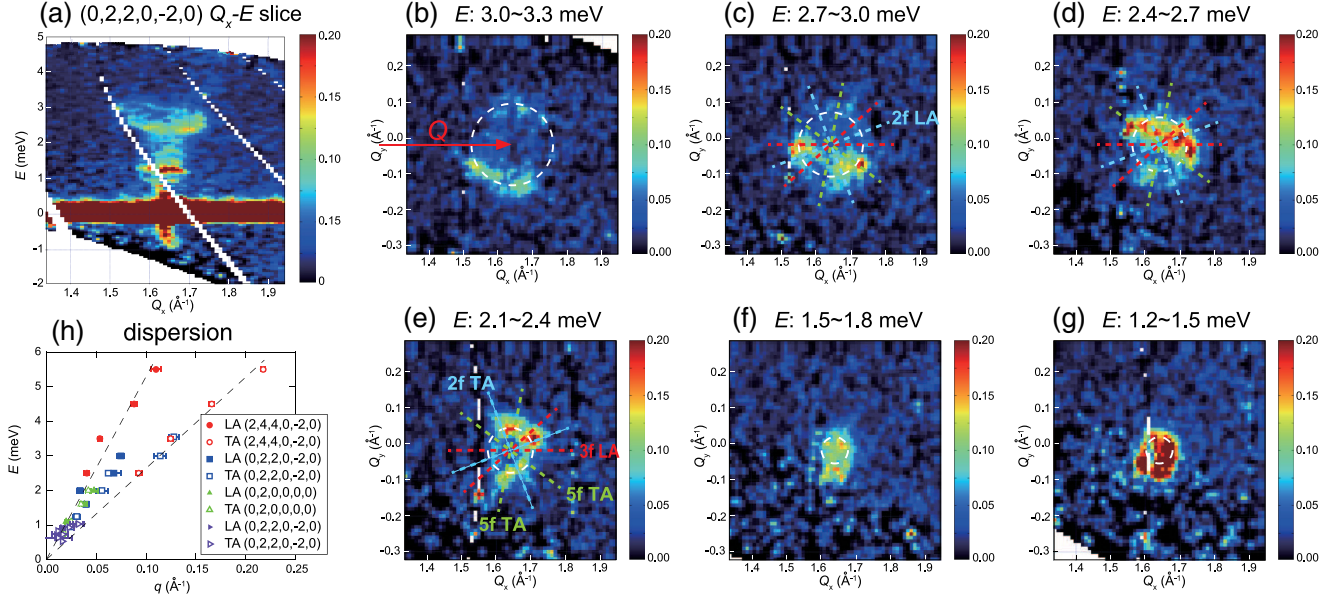


FIG. 2. Contour maps of phonon scattering intensity at a temperature of 300 K around the $(0, 2, 2, 0, -2, 0)$ Bragg peak at $(Q_x, Q_y, Q_z) = (1.64 \text{ \AA}^{-1}, 0, 0)$ obtained using the AMATERAS spectrometer with an ΔE of 0.15 meV. In (a), the Q_x - E slice integrates phonon intensities within the Q region of $|Q_y, Q_z| < 0.1 \text{ \AA}^{-1}$, whereas the Q_x - Q_y slices depicted in (b)–(g) integrate data for $|Q_z| < 0.1 \text{ \AA}^{-1}$ and an energy width of 0.3 meV. (h) Phonon dispersions of the longitudinal (LA) and transverse (TA) acoustic phonons, which were obtained from phonons around several Bragg peaks.

origin of these signals. Suppression of phonon intensities at these energies was commonly observed for other Bragg peaks (Fig. S4 in Supplemental Material [18]). Figures 3(b) and 3(c) show the Q -integrated phonon intensity obtained with finer energy resolutions ($\Delta E = 0.015$ and 0.004 meV, respectively) using the neutron backscattering spectrometer DNA. Finer dip structures were observed in the lower-energy regions at $0.1, \pm 0.2$, and ± 0.4 meV [Fig. 3(b)]. The expected dip at -0.1 meV is filled by asymmetric tail of elastic peak in minus-energy side. These pseudo-gap energies

are roughly scaled by golden mean τ , 0.12, 0.19, 0.31, 0.51, 0.82, 1.33, and 2.15 meV, indicating close relationship to the self-similar structure of quasicrystals. Thus, the current study provides the first direct evidence of the hierarchical pseudo-gap structure in the phonon spectra of quasicrystals. Interestingly, the phonon intensity changes smoothly in the extremely low-energy region below 0.06 meV [Fig. 3(c)], which will be discussed later.

To simulate phonon dispersions in quasicrystal lattices, we calculated phonon dispersions on a one-dimensional

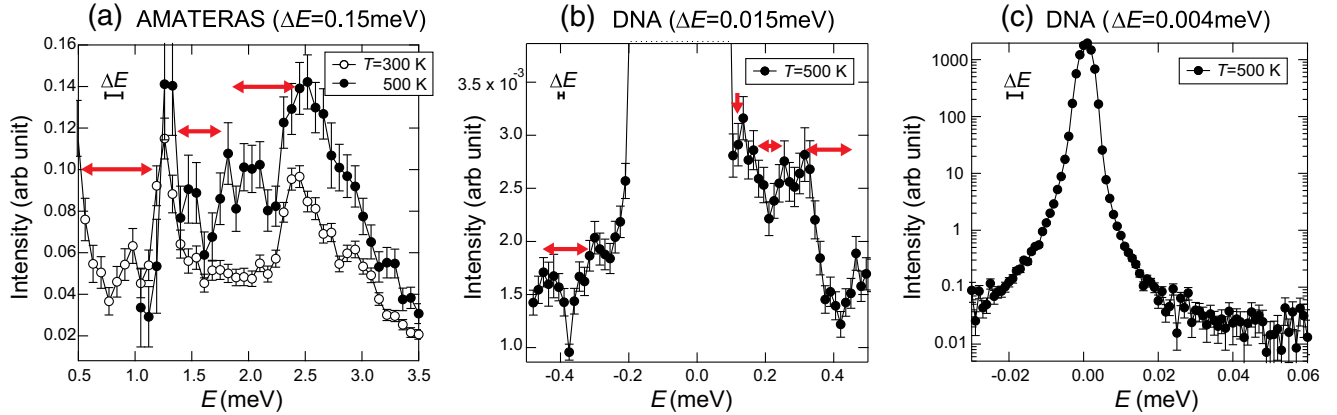


FIG. 3. Energy dependences of Q -integrated phonon intensity around the Bragg peak $(0, 2, 2, 0, -2, 0)$ obtained using (a) AMATERAS with a ΔE of 0.15 meV, (b) DNA with ΔE of 0.015 meV, and (c) DNA with ΔE of 0.004 meV. The ranges of Q integration are $1.525 < Q_x < 1.725$ and $|Q_y, Q_z| < 0.1 \text{ \AA}^{-1}$. The red arrows indicate the pseudo-gap regions (see Table S3 in Supplemental Material [18]).

Fibonacci lattice (high-order approximant with 21 atoms in a unit cell) (Fig. S5 in Supplemental Material [18]). A large gap and finer gaps open at the intersection of acoustic branches that extend linearly from the Bragg points. The gap size is proportional to the square root of Bragg peak intensity $S(Q, 0)$ of the intersecting dispersion. Therefore, relatively large gaps are expected to open at energies scaled by τ because the Q positions of the intense Bragg peaks are scaled by τ in the face-centered i-AIPdMn, which is consistent with the observed pseudo-gaps. Although the current simulations on the high-order approximant cannot reproduce finer pseudo-gaps expected for self-similar structures of quasicrystals, the depth of pseudo-gaps depends on the size of pseudo-gaps and too fine gaps may not be visible with finite ΔE .

In the real three-dimensional quasicrystal i-AIPdMn, the Q position of intense Bragg peaks are slightly different among principal two-, three-, and fivefold axes, and the slopes of the LA mode is steeper than that of the TA mode [24], which gives slightly different pseudo-gap energies as summarized in Tables S2 and S3 in Supplemental Material [18]. Notably, the phonon intensity shown in Fig. 3 was obtained from Q integration of $\pm 0.15 \text{ \AA}^{-1}$ for Q_x and $\pm 0.1 \text{ \AA}^{-1}$ for Q_y and Q_z around the $(0, 2, 2, 0, -2, 0)$ Bragg peak; therefore, the signal below 2.2 meV includes pseudo-gaps of TA and LA modes for all directions. Additionally, owing to the finite ΔE (horizontal bars in Fig. 3), these pseudo-gaps overlap and form pseudo-gap regions, as summarized in Table S3 in Supplemental Material [18]. The suppression of the phonon intensity in Fig. 3 matches well with these pseudo-gap regions indicated by red arrows.

Interestingly, no pseudo-gap structure was observed below 0.06 meV [Fig. 3(c)]. The observed lowest pseudo-gap at 0.10–0.13 meV [Fig. 3(b)] corresponds to the TA modes at $q = 0.0046\text{--}0.0060 \text{ \AA}^{-1}$ and the LA modes at $q = 0.0023\text{--}0.0030 \text{ \AA}^{-1}$. The wave length of these modes can be calculated as $2\pi/q = 1000\text{--}1400$ and $2000\text{--}2700 \text{ \AA}$ for the TA and LA modes, respectively. The degree of structural perfection of i-AIPdMn was investigated by synchrotron x-ray diffractometry and imaging technique [25]. The structural coherence length calculated from the FWHM of Bragg peaks was between 480 and 2000 \AA , depending on the samples, which matches the phonon wavelength of the lowest pseudo-gap. Therefore, the absence of pseudo-gap in extremely low-energy regions could be associated with no pseudo-gaps for wavelengths beyond the coherence length of quasiperiodic order.

In addition to the hierarchical pseudo-gap structure in energy, the Q distribution of the phonon intensity is also significantly different from the normal acoustic phonon modes; they are concentrated in specific directions, and the distribution varies with energy [Figs. 2(b)–2(g)]. Suppression of the phonon intensity along specific directions as indicated by dotted lines can be explained by

anisotropic pseudo-gaps summarized in Table S3 in Supplemental Material [18]. However, Figs. 2(b) and 2(d) show asymmetric phonon intensities in opposite directions with respect to the Bragg point. One of the important differences between periodic lattice and quasicrystals is the existence of the Brillouin zone. In periodic lattices, phonons in a Brillouin zone are essentially not scattered except by defects, coupling to other degrees of freedom, and multiple scattering at high temperatures. Conversely, phonons in quasicrystals can be scattered by the surrounding Bragg peaks, which are often not symmetric.

Asymmetry in phonon intensity was also observed with respect to energy (Fig. 4), which have not been predicted even theoretically. Almost no phonon intensity was observed on the negative-energy side for the E - Q_x slice around $(0, 2, 2, 0, 0, 0)$ [Fig. 4(a)], which can be confirmed in the Q_x - Q_y slices at $-1.2 < E < -0.9$ meV. Phonons are quasiparticles subject to Bose statistics, whose intensity is proportional to the Bose factor $n(\omega) = 1/[\exp(\hbar\omega/k_B T) - 1]$, where k_B is Boltzmann's constant. $n(\omega)$ on the negative-energy side can be close to zero at low temperatures; however, the current data were measured at 300 K, which rules out such a

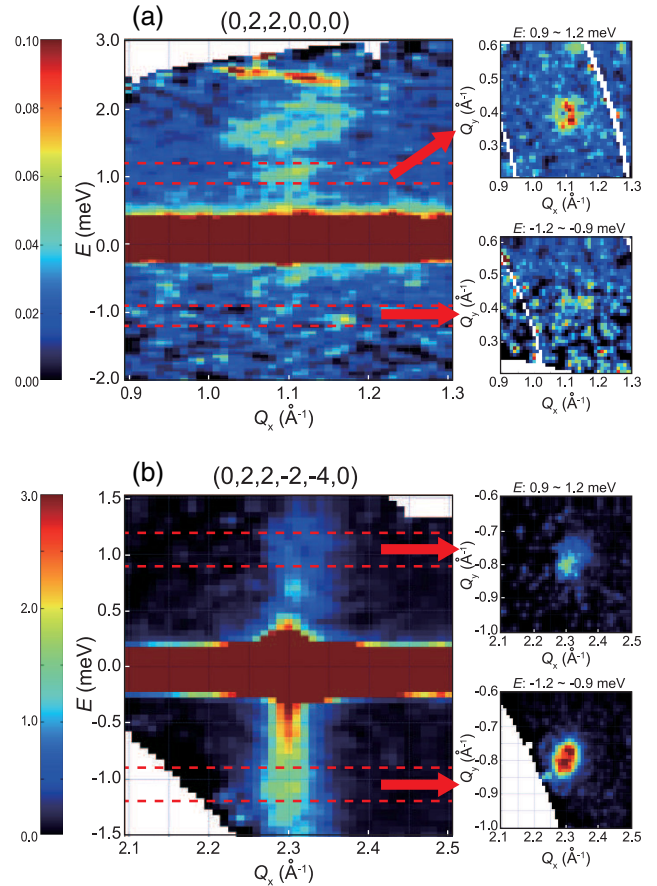


FIG. 4. Asymmetric phonon signal with respect to energy around (a) $(0, 2, 2, 0, 0, 0)$ and (b) $(0, 2, 2, -2, -4, 0)$ Bragg peaks obtained using AMATERAS spectrometer with ΔE of 0.15 meV at $T = 300$ K.

possibility. Conversely, the phonon intensity on the positive-energy side is significantly weaker than that on the negative-energy side around $(0, 2, 2, -2, -4, 0)$ [Fig. 4(b)], which has never been observed in phonon spectra of periodic lattices. Interestingly, similar asymmetric signal between the positive and negative energy was reported in the local electronic DOS of quasicrystal AlPdMn by scanning tunneling microscopy [26].

The principle of detailed balance of scattering function $S(-Q, -\omega) = \exp(-\hbar\omega/k_B T) S(Q, \omega)$ guarantees that excitation at (Q, ω) should have a nearly equivalent signal at $(-Q, -\omega)$ as the $\exp(-\hbar\omega/k_B T)$ factor becomes ~ 1 for low energies (< 3 meV) and $T = 300$ K. For powder samples, which provides averaged phonon intensities of all directions including both $S(Q, \omega)$ and $S(-Q, -\omega)$, symmetric signals are expected to be recovered at $T = 300$ K, which was actually confirmed with the same experimental setup (Fig. S6 in Supplemental Material [18]). In systems with centrosymmetry, the signals at $(-Q, -\omega)$ and $(Q, -\omega)$ are equivalent, resulting in a symmetric signal with respect to energy around Bragg points at Q . In periodic lattices without inversion symmetry, such as chiral MnSi, nonreciprocal phonon dispersions with respect to reduced wave vector $q (= Q - Q_{\text{Bragg}})$ and $-q$ have been revealed [16]. Although structural studies on quasicrystals have been performed assuming inversion symmetry, dynamical three-beam diffraction reported the noncentrosymmetric nature of i-AlPdMn [27]. The current study reveals nonreciprocal phonon dynamics in quasicrystals in terms of intensity between the positive and negative energy, which can be related to the asymmetry in phonon intensity between Q and $-Q$.

The current study reveals the hierarchical pseudo-gap structure in the phonon spectra of quasicrystal i-AlPdMn. Interesting properties such as the asymmetric phonon intensity both in energy and Q were revealed, which are absent in periodic lattices. Because phonons play an important role in thermal, optical, and electrical physical properties of condensed matters, these distinctive properties in the phonons of quasicrystals open the door to functional quasicrystals not being available in periodic lattices.

Acknowledgments—We are grateful to T. J. Sato, H. Takakura, N. Fujita, and S. Watanabe for helpful discussions. We acknowledge beam time awarded by J-PARC (proposals 2020A0094, 2020B0201). M. M. was supported by JSPS KAKENHI Grant No. JP19H05819. K. E was supported by JSPS KAKENHI Grants No. JP19H05821 and JST-CREST Grants No. JPMJCR2203.

- [1] D. Shechtman, I. Blech, D. Gratias, and J. W. Cahn, *Phys. Rev. Lett.* **53**, 1951 (1984).
- [2] P. Lanco, C. Berger, F. Cyrot-Lackmann, and A. Sulpice, *J. Non-Cryst. Solids* **153**, 325 (1993).

- [3] K. Edagawa and K. Kajiyama, *Mater. Sci. Eng.* **294**, 646 (2000).
- [4] A. Pope, T. M. Tritt, M. Chernikov, and M. Feuerbacher, *Appl. Phys. Lett.* **75**, 1854 (1999).
- [5] K. Deguchi, S. Matsukawa, N. K. Sato, T. Hattori, K. Ishida, H. Takakura, and T. Ishimasa, *Nat. Mater.* **11**, 1013 (2012).
- [6] K. Kamiya, T. Takeuchi, N. Kabeya, N. Wada, T. Ishimasa, A. Ochiai, K. Deguchi, K. Imura, and N. Sato, *Nat. Commun.* **9**, 154 (2018).
- [7] T. Janssen, *Acta Crystallogr. Sect. A* **42**, 261 (1986).
- [8] A. Yamamoto, *Acta Crystallogr. Sect. A* **52**, 509 (1996).
- [9] A. Yamamoto, H. Takakura, and A. P. Tsai, *Phys. Rev. B* **68**, 094201 (2003).
- [10] A. Sütő, *J. Stat. Phys.* **56**, 525 (1989).
- [11] K. Niizeki and T. Akamatsu, *J. Phys. Condens. Matter* **2**, 2759 (1990).
- [12] T. Janssen, G. Chapuis, and M. d. Boissieu, *Aperiodic Crystals: From Modulated Phases to Quasicrystals* (Oxford University Press, New York, 2002).
- [13] M. De Boissieu, M. Boudard, R. Bellissent, M. Quilichini, B. Hennion, R. Currat, A. Goldman, and C. Janot, *J. Phys. Condens. Matter* **5**, 4945 (1993).
- [14] M. Boudard, M. De Boissieu, S. Kycia, A. Goldman, B. Hennion, R. Bellissen, M. Quilichini, R. Currat, and C. Janot, *J. Phys. Condens. Matter* **7**, 7299 (1995).
- [15] M. De Boissieu, S. Francoual, M. Mihalkovič, K. Shibata, A. Q. Baron, Y. Sidis, T. Ishimasa, D. Wu, T. Lograsso, L.-P. Regnault *et al.*, *Nat. Mater.* **6**, 977 (2007).
- [16] Y. Nii, Y. Hirokane, T. Koretsune, D. Ishikawa, A. Q. R. Baron, and Y. Onose, *Phys. Rev. B* **104**, L081101 (2021).
- [17] J. Zhang, Y. Kamimura, Y. Tokumoto, and K. Edagawa, *Philos. Mag.* **102**, 1461 (2022).
- [18] See Supplemental Material at <http://link.aps.org/supplemental/10.1103/PhysRevLett.133.136101> for the details of the neutron Laue diffraction, indices of Bragg peaks, common gap features, simulation of phonon dispersions, and powder averaged phonon intensity.
- [19] V. Elser, *Phys. Rev. B* **32**, 4892 (1985).
- [20] K. Nakajima, S. Ohira-Kawamura, T. Kikuchi, M. Nakamura, R. Kajimoto, Y. Inamura, N. Takahashi, K. Aizawa, K. Suzuya, and K. Shibata, *J. Phys. Soc. Jpn.* **80**, SB028 (2011).
- [21] K. Shibata, N. Takahashi, Y. Kawakita, M. Matsuura, T. Yamada, T. Tominaga, W. Kambara, M. Kobayashi, Y. Inamura, T. Nakatani *et al.*, *J. Phys. Soc. Jpn. Conf. Proc.* **8**, 036022 (2015).
- [22] Y. Inamura, T. Nakatani, J. Suzuki, and T. Otomo, *J. Phys. Soc. Jpn.* **82**, SA031 (2011).
- [23] M. de Boissieu, *Chem. Soc. Rev.* **41**, 6778 (2012).
- [24] Y. Amazit, M. De Boissieu, and A. Zarembowitch, *Europhys. Lett.* **20**, 703 (1992).
- [25] J. Gastaldi, S. Agliozzo, A. Letoublon, J. Wang, L. Mancini, H. Klein, J. Härtwig, J. Baruchel, I. R. Fisher, T. Sato *et al.*, *Philos. Mag.* **83**, 1 (2003).
- [26] R. Widmer, P. Gröning, M. Feuerbacher, and O. Gröning, *Phys. Rev. B* **79**, 104202 (2009).
- [27] Y. Zhang, R. Colella, Q. Shen, and S. Kycia, *Acta Crystallogr. Sect. A* **54**, 411 (1998).